

# A perforated diamond anvil cell for high-energy x-ray diffraction of liquids and amorphous solids at high pressure

Emmanuel Soignard,<sup>1</sup> Chris J. Benmore,<sup>2,3</sup> and Jeffery L. Yarger<sup>4,2,a)</sup>

<sup>1</sup>*LeRoy Eyring Center for Solid State Science, Arizona State University, Tempe, Arizona 85287, USA*

<sup>2</sup>*Department of Physics, Arizona State University, Tempe, Arizona 85287, USA*

<sup>3</sup>*X-ray Science Division, Advanced Photon Source, Argonne National Laboratory, Argonne, Illinois 60439, USA*

<sup>4</sup>*Department of Chemistry and Biochemistry, Arizona State University, Tempe, Arizona 85287, USA*

(Received 18 November 2009; accepted 15 February 2010; published online 29 March 2010)

Diamond anvil cells (DACs) are widely used for the study of materials at high pressure. The typical diamonds used are between 1 and 3 mm thick, while the sample contained within the opposing diamonds is often just a few microns in thickness. Hence, any absorbance or scattering from diamond can cause a significant background or interference when probing a sample in a DAC. By perforating the diamond to within 50–100  $\mu\text{m}$  of the sample, the amount of diamond and the resulting background or interference can be dramatically reduced. The DAC presented in this article is designed to study amorphous materials at high pressure using high-energy x-ray scattering ( $>60$  keV) using laser-perforated diamonds. A small diameter perforation maintains structural integrity and has allowed us to reach pressures  $>50$  GPa, while dramatically decreasing the intensity of the x-ray diffraction background (primarily Compton scattering) when compared to studies using solid diamonds. This cell design allows us for the first time measurement of x-ray scattering from light (low  $Z$ ) amorphous materials. Here, we present data for two examples using the described DAC with one and two perforated diamond geometries for the high-pressure structural studies of  $\text{SiO}_2$  glass and  $\text{B}_2\text{O}_3$  glass. © 2010 American Institute of Physics.

[doi:[10.1063/1.3356977](https://doi.org/10.1063/1.3356977)]

## I. INTRODUCTION

Diamond anvil cells (DACs) have now been used for over 50 years to study materials *in situ* at high pressure.<sup>1–4</sup> With the availability of high brightness microfocused synchrotron x-ray beams, x-ray diffraction (XRD) studies of crystalline samples within the DAC have become routine.<sup>3,5,6</sup> The use of higher energy ( $>60$  keV) has allowed large  $Q$ -space data collection and the accurate measurement of diffuse scattering from amorphous materials.<sup>7–9</sup> In recent years, high-energy DAC XRD has been extended to liquids and amorphous solids at high pressure.<sup>10–25</sup>

In a typical ambient pressure XRD experiment on liquids or amorphous solids, millimeter size samples are either free-standing or contained within thin walled capillaries. The sample volume and signal are considerably larger than that of the container. The signal from the empty container can be measured prior to loading the sample and the signal from the container subtracted from the measured pattern of the filled capillary with negligible attenuation effects, to give rise to a background free sample scattering pattern. Another important advantage of standard thin walled glass or polyimide tube sample holder is the absence of obstructions in the path of the scattered beam. For heavy elements, the signal can, in principle, be measured over a  $2\theta=120^\circ$  range, giving access to momentum transfers  $Q=4\pi \sin \theta/\lambda$  in excess of  $50 \text{ \AA}^{-1}$ .

In a DAC, the sample is extremely small with respect to

the sample container. Each diamond anvil typically has a height of 1–3 mm and the sample is, in general,  $<50 \mu\text{m}$  thick. The single crystal diamonds give rise to a large background when compared to the weak diffuse scattering from the amorphous sample. As pressure is increased, the gasket deforms and becomes thinner, resulting in a progressive change in the background arising from the diamond anvils. The pressure dependent background changes make the data correction problematic for weakly scattering samples such as oxides. Another limitation of scattering experiments in the DAC is the limited opening of the backing plates, typically restricted to  $2\theta \sim 25 \pm 5^\circ$  (see Fig. 1). This angular restriction limits the accessible maximum  $Q$  to  $\sim 17.5 \text{ \AA}^{-1}$  at 80 keV.

Few structural studies of amorphous materials at high-pressure measured to high momentum transfer are reported in literature.<sup>12,15,18,20</sup> The method used in most of the published work has two limitations: either the pressure is limited to less than 15 GPa due to limited structural integrity of the mechanically ground perforated anvils<sup>18</sup> or the experiment is performed using energy dispersive techniques.<sup>14</sup> Energy dispersive experiments benefit from much greater flux compared to the monochromatic measurements described here; however the attenuation, geometrical, and multiple scattering corrections are considerably larger and dramatically more complex, making absolute normalization difficult. In order to improve the accessible pressure range, while maintaining the large accessible  $Q$  range using very high-energy

<sup>a)</sup>Electronic mail: [jyarger@gmail.com](mailto:jyarger@gmail.com).

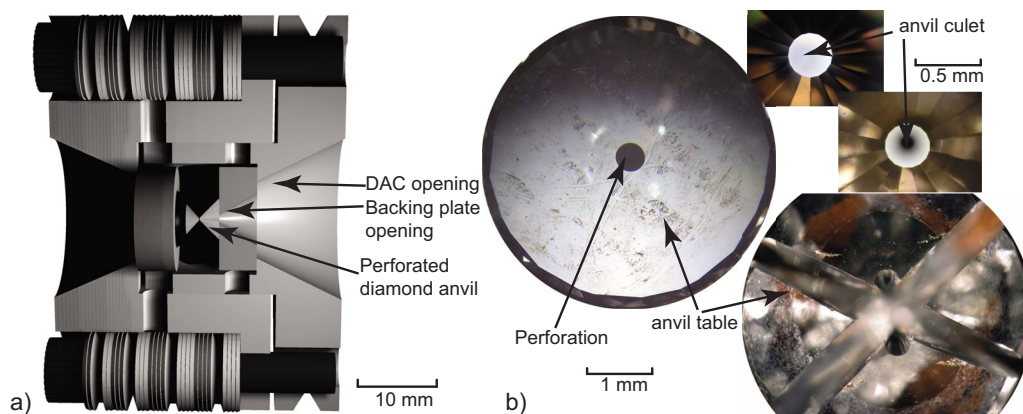


FIG. 1. (Color online) (a) The illustration on the right shows the opening of the cell and the backing plate for a typical symmetrical cell. (b) Photograph of a laser-perforated diamond table (top left), view of the culet with and without transmitted light (top right). At the bottom right is a photograph of a broken perforated anvil used with insufficient support.

(>60 keV) monochromatic x-rays, we have used laser-drilled diamonds with a very small opening angle. The perforation typically reaches within 50–100  $\mu\text{m}$  of the culet surface. These perforated diamonds are designed to maintain structural integrity and results in DACs that can reach pressures of 40–50 GPa, reproducibly.

In the first part of this article, we will describe the cell designs and the changes resulting from the use of zero, one or two perforated diamonds. We will then discuss the optimal way to perform the data corrections and discuss the optimal choice of DAC for a given experiment. Finally, we will illustrate the use of our cell design and data correction with two examples of data reduction for high-energy XRD patterns measured in the DAC. The first example will be for a sample of  $\text{SiO}_2$  glass *in situ* at 43.5 GPa measured in a cell assembled with one solid and one perforated diamond. The second example will be a sample of  $\text{B}_2\text{O}_3$  glass measured *in situ* at 16 GPa in the DAC with two perforated diamonds.

## II. CELL DESIGN

The perforated DAC has been optimized to measure high-energy XRD from low atomic weight materials (low  $Z$ ), such as  $\text{BeF}_2$  or  $\text{B}_2\text{O}_3$ . The perforated diamond backgrounds, cell materials, and a discussion about the diamond alignment are given below.

### A. Diamond perforation

The diamond perforation was drilled using a high power YAG (yttrium aluminum garnet) laser (Almax Industries, Diksmuide, Belgium<sup>26</sup>). The conical opening angle is very narrow with an opening diameter on the table ranging from 0.4 to 1 mm. The end of the perforation is within less than 50–200  $\mu\text{m}$  of the culet. In Fig. 1, the diameter of the perforation on the table is 400  $\mu\text{m}$  and less than 50  $\mu\text{m}$  near the culet. In Fig. 1(b), the dark area on the photograph of the culet shows that the light is not being transmitted through the perforation. The anvil design shown in Fig. 1(b) is a modified brilliant cut type IA diamond with the table cut along the (100) plane with a 300  $\mu\text{m}$  culet diameter. The table of the diamond is lowered to increase its diameter to 4.2 mm.

Figure 2 shows the background for a cell with an empty rhenium gasket assembled using four different geometries. The cell can be loaded with any combination of solid or perforated diamonds. It is clear from Fig. 2 that the cell assembled with two perforated diamonds has dramatically lower background intensity than the cell with two solid diamonds. There is a sixfold increase in background intensity at 9  $\text{\AA}^{-1}$  between a cell assembled with two perforated diamonds and a cell assembled with two solid diamonds. In comparison, the two cells loaded with one perforated diamond and one solid diamond have intermediate background intensity. The background of the cell with the perforation on the downstream side of the cell has a lower background compared to the one with the perforation on the upstream side of

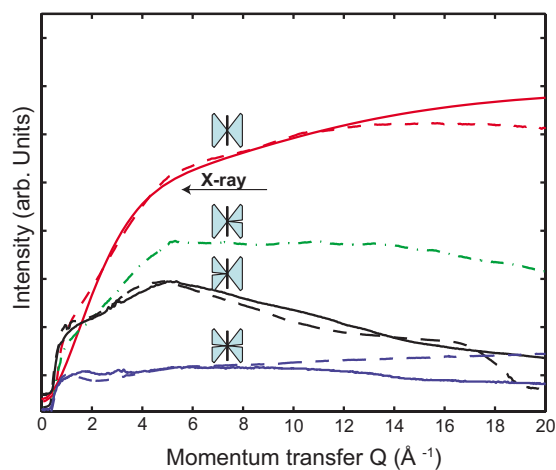


FIG. 2. (Color online) The background signals from four different anvil cell setups are shown. The dashed lines (----) are for data collected at 80 keV for diamonds mounted on Be backing plates and the solid lines (—) are for data collected at 100 keV for anvils mounted on c-BN plates. The highest dashed line (----) plotted is for the cell loaded with two solid anvils, which is reasonably approximated by the overlapping solid line of the Compton scattering of carbon. The three intermediate curves are from cells loaded with one perforated diamond anvil and one solid anvil. The dash-dotted (-.-) curve represents the background with the diamond on the upstream side of the cell at 80 keV and the third set of lines from the top are for a cell with the perforated diamond on the downstream side. The experimental setups with the lowest background intensity are the ones loaded with two perforated diamond anvils.

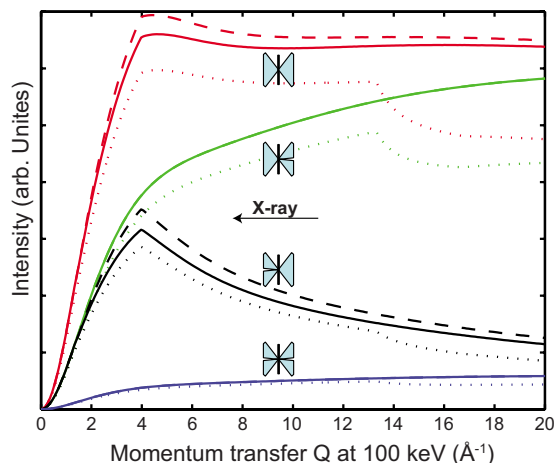


FIG. 3. (Color online) Plots of the estimated change in backgrounds from highest to lowest intensity at  $Q=20 \text{ \AA}^{-1}$  for two nonperforated diamonds (top set of lines), one perforated diamond on the upstream and one nonperforated on the downstream side of the cell (second set from the top), one perforated diamond on the downstream side of the cell and one perforated diamond on the upstream side of the cell (third set from the top), and two perforated diamonds (lowest intensity set of lines). Three curves are plotted for each setup. The solid line (—) is for the DAC before compression (hole diameter of  $100 \mu\text{m}$  and a  $30 \mu\text{m}$  thick indent), the dashed line (---) is modeled for a DAC at high-pressure (hole diameter of  $80 \mu\text{m}$  and  $10 \mu\text{m}$  thick indent), the dotted curve (····) is the result of the combination of the solid curve with the absorption of the diamond and backing plate taken into account.

the cell. This is understood by recognizing that the rhenium gasket and the cell body itself absorb part of the scattering from the upstream anvil at high angles. For experiments using soft x-rays,<sup>27–29</sup> the perforation is primarily used to reduce the absorption of the sample signal by the diamond anvils. However, above 30 keV, the x-ray transmission through the diamond anvil ( $\sim 1.9 \text{ mm}$  thick) is  $>80\%$ .<sup>30</sup> Hence, in high-energy XRD, the perforation is not used to minimize x-ray absorption; rather its primary purpose is to reduce the Compton scattering originating from the diamond anvils. We have modeled the various cell assembly with both perforated and nonperforated diamonds assuming that the background solely results from the Compton scattering of diamond (Fig. 3). The backgrounds were calculated using a diamond thickness of  $1.9 \text{ mm}$  with an initial rhenium gasket thickness of  $30 \mu\text{m}$  and a hole diameter of  $100 \mu\text{m}$ . Compression is simulated by reducing the sample thickness to  $10 \mu\text{m}$  with a hole diameter of  $80 \mu\text{m}$ . The perforation diameter is assumed to have a larger diameter than the x-ray beam. The x-ray beam is assumed to have a negligible diameter compared to the other dimensions in the model. The curve in Fig. 3 was generated by integrating the intensity as a function of distance ( $d$ ) from the table of the upstream diamond to the table of the downstream diamond along the direct x-ray beam axis. The intensity as a function of angle for each  $\delta d$  was calculated taking into account the absorption resulting from the distance the Compton signal traveled through each of the materials (rhenium and diamond). In the model, the perforation(s) is assumed to be  $100 \mu\text{m}$  from the culet of the diamond. As shown in Fig. 3, there is very good agreement between the observed and calculated backgrounds, indicating that the background indeed originates

primarily from the Compton scattering of diamond. The background generated from two solid diamonds has an intensity 3.4 times larger than that generated by a cell with one solid diamond on the upstream side and one perforated diamond on the downstream side, which also has a background four times larger than the background generated by the model with a cell with the two perforated diamonds at  $9 \text{ \AA}^{-1}$ . The use of small diameter perforation from the model clearly presents a dramatic decrease in the background intensity originating from the Compton scattering from the diamond anvils, which in turn provides a dramatic improvement in data analysis.

The coherent scattering from diamond mainly gives rise to very intense Bragg reflections (typically from 004 and 220 families) and some weaker diffuse scattering. The diffuse scattering is relatively weak and does not appear to have a noticeable impact on the data analysis. When setting up the experiment, the intensity of the Bragg spots from the single crystal diamonds should be minimized by slightly rotating the cell ( $<0.5^\circ$ ) to avoid saturating the detector and to minimize the blooming onto other pixels of the detector. The single crystal diamond Bragg peaks are relatively discrete in space and can be removed from the two-dimensional (2D) diffraction data using the following relatively simple image processing procedures. For a homogeneous powder material or amorphous material, all the azimuths of the diffraction pattern should be identical. This property does not hold true for highly textured and in particular single crystal materials such as our diamond anvils. If we plot a vertical stack to form a 2D diffraction pattern of  $Q$  as a function of azimuth (called a “cake” image in the freely available software program FIT2D),<sup>31</sup> the result should be a figure where each point for a given column has the same intensity. In the case of a pattern combining single crystals (diamond anvils) and amorphous material (our glass sample), the columns will be a combination of even intensity lines and discrete, very high, intensity spots. Using that property of the azimuth projection, we determine the intensity distribution along the columns and reject pixels with intensities outside a chosen range from the median intensity. That simple procedure rejects all of the Bragg spots (both weak and intense) from the background-subtracted diffraction pattern. The diamond perforation as shown in Fig. 1 dramatically decreases the intensity of the broad background as well as the intensity of the diamond Bragg reflections.

## B. Wide diffraction angle and high energy

The diffraction pattern is measured in reciprocal ( $Q$ ) space and a Fourier transform is typically used to convert reciprocal space to real space data. However, this transformation convolutes sinc oscillations with the data due to truncation effects resulting in artificial peak broadening.<sup>32</sup> It is a common practice to use an apodization function in order to force damping of the signal in a continuous fashion, which further broadens the real space spectra. In order to obtain accurate real space transforms of amorphous structure, it is imperative to have data up to large  $Q$  values (typically  $>20\text{--}30 \text{ \AA}^{-1}$ ) in order to maximize the resolution in real

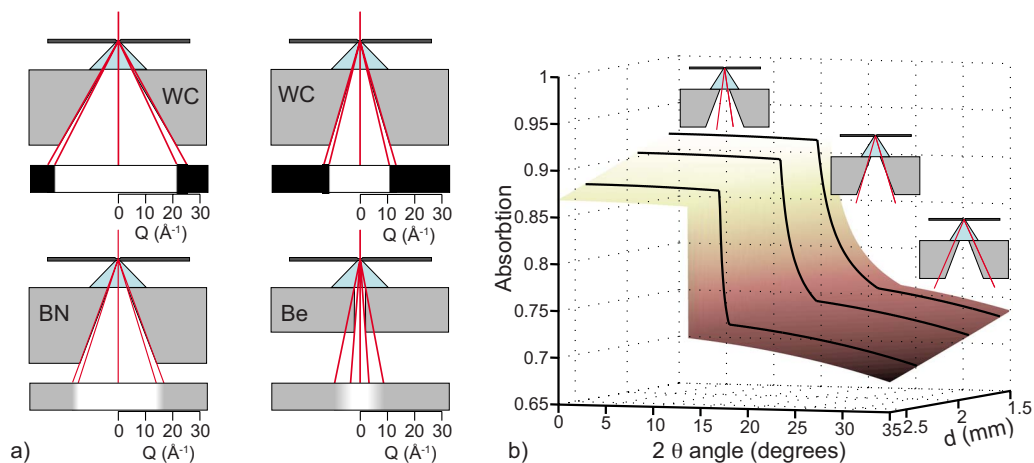


FIG. 4. (Color online) (a) Sketch of a 1.9 mm thick diamond mounted on three types of backing plates; the top two are tungsten carbide and the bottom one is a boron nitride backing plate and a thinner Be backing plate, the lines indicate the direct x-ray beam and selected diffracted beam. The gray scale plot below each assembly indicates the attenuation from the diamond and the backing plate at 100 keV. (b) Plot of the x-ray absorption at 100 keV as a function of scattering angle and diamond thickness for a cubic boron nitride backing plate (Ref. 30).

space. Leadbetter and Wright<sup>32</sup> showed that with a decreasing  $Q$ -range, the error on the coordination number dramatically increases.

In order to access the largest possible  $Q$  range, it is necessary to maximize the accessible diffraction angle (while still achieving a reasonably small minimum  $Q$  value  $<1 \text{ \AA}^{-1}$ ) and maximize the energy. For example, given a maximum  $2\theta$  of  $25^\circ$ , at 30 keV the maximum  $Q$  is  $6.6 \text{ \AA}^{-1}$  whereas at 100 keV the maximum  $Q$  is  $21.9 \text{ \AA}^{-1}$  (at 80 keV the maximum  $Q$  would be  $17.5 \text{ \AA}^{-1}$ ). Typically, amorphous diffraction is performed at high energies ( $>60 \text{ keV}$ ) to minimize multiple scattering and attenuation effects, and increase the  $Q$ -range. This is done mainly at the expense of flux and detector efficiency. The XRD data shown in this paper were all taken at Argonne National Laboratory (ANL) at the Advanced Photon Source (APS) using the microfocused beamline 1-ID-C with energies of either 80 or 100 keV and a beam size of  $40 \times 40 \text{ \mu m}^2$ . Both energies are acceptable, although 100 keV is preferred for high-pressure DAC studies ( $>10 \text{ GPa}$ ) with narrow exit geometries since it gives access to a larger  $Q$ -range ( $21.9 \text{ \AA}^{-1}$  at 100 keV versus  $17.5 \text{ \AA}^{-1}$  at 80 keV). Only a few synchrotron facilities produce high brightness submillimeter monochromatic x-ray beams at energies of 60 keV and higher, among those are beamline ID15 at ESRF in France and BL04B2 at Spring 8 in Japan.<sup>33</sup>

Although the flux of high-energy x-ray beamlines is considerably lower than those at lower energies, high-pressure diffraction experiments have been made possible in recent years through the development and use of large area detectors.<sup>34</sup> High-pressure experiments on glasses and liquids using 1-ID-C at APS have been performed using Mar345 image plates and General Electric and Perkin Elmer a-Si flat plate detectors. In general, the a-Si flat plate detectors are preferred due to their greater efficiency at higher energies compared to image plates. However, these detectors have inherently large dark currents, which can be effected by changes in temperature. This effect can be minimized by taking repeated dark current measurements with the beam off

throughout the experiment and water cooling the detector to keep the temperature uniform and stable.

### C. Backing plate and cell assembly

The diamond perforation is the primary source for mechanical weakness of the anvil and can result in the splitting along the (110) cleavage plane, as shown in Fig. 1. In order to prevent splitting of the perforated anvil it is critical to mount the anvil on a strong support, minimizing the deformation of the anvil's table. In a typical high-pressure experiment, the diamond anvils are mounted on tungsten carbide backing plates.

Depending on the diffraction geometry of the experiment, we used tungsten carbide (WC), beryllium (Be), or cubic boron nitride (BN) backing plates [Fig. 4(a)]. The WC backing plate is not x-ray transparent (absorbs over 99.5% of the x-rays at 100 keV within 1.5 mm). The typical dimensions used for the wide opening WC backing plate have an opening of 2 mm diameter on the diamond side and a cone angle of  $61^\circ$  allowing data collection of up to  $24^\circ$  in  $2\theta$  for a 1.9 mm high diamond. Our attempts to use a wide opening WC backing plate to support the perforated diamond resulted in the splitting of the anvil, as shown in Fig. 1. The anvil table deformed with increasing uniaxial force and the lack of confining forces placed the anvil in tension resulting in the failure along the (110) cleavage plane. Consequently, the wide opening WC backing plate can only be used to support nonperforated solid diamonds. Alternative backing plate materials are Be and BN, which are both x-ray transparent with x-ray attenuation coefficients comparable to that of diamond [see Fig. 4(a)]. The transparency of the support no longer requires a wide opening and allows for a small physical opening angle while providing strong support of the perforated anvil. We used both BN and Be backing plates successfully to support perforated anvils to pressures beyond 43 GPa. The BN backing plates used in the experiment had a conical opening resulting in a convoluted absorption correction [Fig. 4(b)]. The absorption curve changed with diamond

thickness, as illustrated in Fig. 4(b). The Be backing plate has a narrow cylindrical opening, and as a result, only the very low angle part of the pattern would be collected without the scattered signal being partially absorbed by the backing plate [Fig. 4(a)].

### III. DATA CORRECTION

In order to process the data properly, it is important to collect data from several background contributions. Because of the vanishing intensity of the x-ray atomic form factors at high  $Q$ , it is crucial to have a very careful correction of the cell background to the highest  $Q$  possible. Mei *et al.*<sup>15</sup> described the standard analysis for obtaining a pseudonuclear structure factor  $S(Q)$  from high-pressure XRD data using the following equation:

$$S(Q) - 1 = \left( \beta \frac{I_s(Q) - A(Q)I_B(Q)}{K(Q)} - \sum_i c_i f_i^2(Q) - \sum_i c_i C_i(Q) \right) / \left[ \sum_i c_i f_i(Q) \right]^2. \quad (1)$$

$I_s(Q)$  is the intensity observed on the detector and is a combination of the sample and the background intensities.  $I_B(Q)$  is the background intensity of the empty DAC.  $A$  and  $K$  are angle dependent attenuation factors.  $\beta$  is a coefficient used to scale the data to the sum of the self-scattering plus Compton scattering  $\sum_i c_i f_i^2(Q) + \sum_i c_i C_i(Q)$ . In the formula,  $c_i$  is the concentration of atomic species  $i$  and  $f_i$  represents the atomic form factor. We demonstrate below that the background intensity  $I_B(Q)$  changes with pressure and a  $Q$  dependent absorption correction  $A(Q)$  can be applied to correct for the backing plate absorption.

#### A. Background correction

##### 1. Background as a function of pressure

In a DAC experiment, the decreasing sample volume (height and diameter) results in the increase in the sample pressure. This very principle makes the background correction at high pressure challenging. Upon increasing the pressure in a DAC, the thickness of the gasket and sample decreases. The thinning of the gasket is not only due to the compression of rhenium but also to the flow of the gasket material from between the diamonds to the outer perimeter of the culet. This transformation results in a variation in the absorption by the gasket of the Compton scattering and diffraction peaks from the upstream diamond. The result is a change in the shape of the background with pressure. Figure 5 shows an example of cell backgrounds collected with the same empty rhenium gasket before compression and after decompression of a SiO<sub>2</sub> glass sample loaded in a DAC with one solid diamond and one perforated diamond on the upstream side, and the downstream side to 35 and 43.5 GPa, respectively. Figure 5 shows that the background intensity change before and after compression from a cell assembled with a perforated diamond on the upstream side and a solid diamond on the downstream side is much smaller than it is for a cell assembled with a solid diamond on the upstream side and a perforated diamond on the downstream side. This

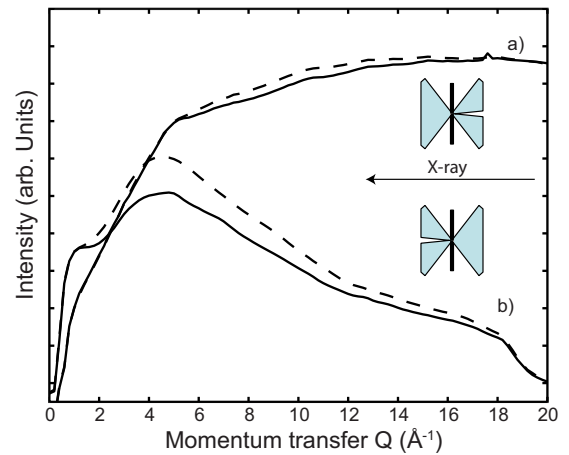


FIG. 5. (Color online) Plots showing the change in background for an empty DAC before compression (—) and after decompression from beyond 35 GPa. The cells were loaded (a) with the perforation on upstream side and (b) with the perforated diamond on the downstream side in both experimental setups, the opposite anvil was nonperforated.

observation is the direct result of the fact that the background intensity generated by a perforated diamond is much weaker than the one generated by a solid diamond. Below we show the example of the analysis of a SiO<sub>2</sub> glass sample at 43.5 GPa with the perforated diamond on the downstream side of the cell. A combination of backgrounds collected with the empty rhenium gasket before compression and after decompression of the cell and removal of the sample is required in order to correct the data. The linear combination of the two backgrounds is used to generate a first order approximation of the background for the correction of data collected at any pressure. This allows us to write the background intensity  $I_B(Q)$  as a linear combination of two spectra,

$$I_B(Q) = x \times I_{B_0}(Q) + (1 - x) \times I_{B_{\text{dec}}}(Q), \quad (2)$$

where  $I_{B_0}(Q)$  is the background of the empty cell with a gasket before compression and  $I_{B_{\text{dec}}}(Q)$  is the background of the empty cell with the gasket after decompression and removal of the sample.

In Fig. 3, we show the changes in the modeled backgrounds. If the upstream diamond is perforated and therefore generates only a weak Compton background, the background does not change noticeably with hole diameter and gasket thickness (the two lines overlap in Fig. 3). However, with a nonperforated upstream diamond, the background changes significantly when the hole diameter and the gasket thickness change, the largest difference is around 4 Å<sup>-1</sup>. Shen *et al.* described a DAC experimental setup using two solid diamonds and an x-ray transparent boron epoxy gasket. The authors showed that using their setup, the background of the diffraction pattern remains constant with pressure. The use of the x-ray transparent gasket described by Shen *et al.*<sup>19</sup> is a reasonable approach when using a solid diamond on the upstream side. However, if a perforated diamond is used on the upstream side, the background changes with pressure will be negligible whether the gasket material is a boron/epoxy gasket or a rhenium gasket. One major drawback of using an x-ray transparent gasket is the difficulty of aligning the sample. In particular, at high energy it is nearly impossible to

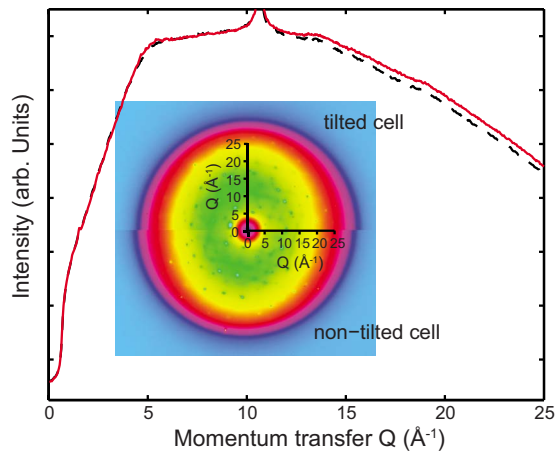


FIG. 6. (Color online) Plot of the measured background intensity as a function of  $Q$  for a thin horizontal slice (10 pixels high) from the 2D diffraction patterns shown in the middle of the figure. The dashed line (----) is the 1D plot of the data for the cell rotated off-axis by  $5^\circ$  and the solid line (—) is a plot of the 1D data for the cell perpendicular to the x-ray beam. The curves are the sum of the left hand and right hand side of the image. Only one-half of each 2D diffraction pattern are shown, the bottom half is from the 2D diffraction pattern of the perpendicular (nontilted) cell and the top half is that of the 2D pattern collected with the cell rotated by  $\sim 5^\circ$ .

discriminate between the light sample and the transparent gasket material. A  $30\ \mu\text{m}$  thick gasket made from high  $Z$  material such as Re absorbs about 25% of the x-ray beam intensity while the sample only absorbs a few percent at 100 keV, providing enough contrast to align the sample into the beam.

## 2. DAC alignment

A small rotation of the DAC will result in a change in the background and signal intensity at high  $Q$ . This is enhanced for perforated diamonds due to the strong geometrical effects (Fig. 6). The pseudonuclear formalism given in Eq. (1) dramatically amplifies the signal at high  $Q$ . Consequently, the differences at high  $Q$  should be carefully corrected. It is important to keep the cell as close to perpendicular to the direct beam as possible in order to minimize the change in background at high  $Q$ . Figure 6 illustrates the changes between a cell perfectly perpendicular (within less than  $1^\circ$ ) to the beam and one slightly rotated by about  $5^\circ$ . The changes in the 2D diffraction pattern are difficult to observe since they occur mostly at high  $Q$  and are relatively weak. However, in the radially integrated one-dimensional (1D) plots there is a large difference in the two backgrounds. The changes in integrated data between the pattern of a cell perpendicular to the beam and the rotated cell are manifested by a monotonous decrease in the background intensity above a threshold momentum transfer value,  $Q$ . Therefore, if the cell slowly moves during the experiment or needs to be rotated due to a change in the diamond diffraction intensity, it is possible to correct the intensity of the background by applying a linear correction to the high  $Q$  part of the pattern.

Empirically, we find that the background intensity  $I_B(Q)$  can then be written as follows:

$$Q \leq Q_a, \quad I_B(Q) = I_B(Q), \quad (3)$$

$$Q \geq Q_a, \quad I_B(Q) = I_B(Q) + \alpha(Q - Q_a),$$

where  $Q_a$  is the momentum transfer above which the cell starts shadowing some of the signal and  $\alpha$  is the slope of the additional Compton scattering due to the rotation of the cell.

## B. Absorption correction

We previously described that one of the optimal diffraction geometries utilizes an x-ray “transparent” backing plate. However, the backing plate is not perfectly x-ray transparent and absorbs part of the x-ray intensity. Since part of the diffraction pattern is collected through the backing plate and part is not, it is critical to perform an accurate absorption correction in order to be able to use the data at  $Q$ -values larger than the physical opening angle of the c-BN or Be backing plate. The correction is performed by using the background collected before or after the experiment with and without the downstream diamond. The correction assumes that the variation of the signal intensity originating from the downstream diamond is not significant over the range where the backing plate absorption varies dramatically. This assumption is reasonable since the downstream diamond is perforated and only generates a small amount of Compton scattering. As shown in Fig. 4, the absorption profile changes with diamond thickness. In a similar fashion, the absorption profile will also change with sample thickness. The  $Q$ -position of the steep change in absorption curve will shift with the distance between the culet of the upstream diamond and the backing plate of the downstream diamond. It is therefore critical to minimize the absolute change in sample thickness when using a c-BN backing plate. Even for low-pressure experiments, the gasket should be indented enough to reduce the plastic flow of the gasket material. The typical indentation thickness of a  $250\ \mu\text{m}$  thick rhenium gasket is about  $30\text{--}40\ \mu\text{m}$  for experiments up to 50 GPa using diamonds with  $300\ \mu\text{m}$  diameter culet. When the absorption correction is required,  $I_S(Q)$  in Eq. (1) becomes

$$I_S(Q) = T_{\text{bp}}(Q) \times I_{\text{obs}}(Q), \quad (4)$$

where  $T_{\text{bp}}(Q)$  is the transmission through the backing plate and  $I_{\text{obs}}(Q)$  is the measured signal on the detector.

## IV. DESIGN CHOICES

The diamond perforation is not perfectly transparent. The perforation is machined using a laser and the laser drilling does not leave a polished surface deep inside the diamond (see Fig. 1). As a consequence, it is not possible to clearly see the culet through the table of the diamond. Diamond alignment is typically performed by first laterally aligning the diamonds looking at the cell from the side. Once aligned, the diamond culets are then brought together and the culet is observed through the table in order to check if the diamond culets are parallel.<sup>35</sup> When using two perforated diamonds, this last step is not possible and therefore the parallel alignment of the diamonds is challenging and currently limits the accessible pressure range with the current DAC technology. The perforation in both diamonds impairs the

visual observation of the sample loading quality and the behavior of the sample chamber with pressure. For example, a sample of amorphous  $\text{BeH}_2$  was compressed to  $\sim 20$  GPa at which pressure the gasket failed, resulting in the destruction of one of the diamonds. A later analysis of the alignment (transmission) scans performed using the x-ray beam indicated that the sample chamber was very slowly expanding. If it were possible to look at the sample under the microscope, the gasket failure could have been avoided. If we could polish the inner part of the drilled diamond the alignment of cells with two perforated diamonds would become a routine as aligning DACs with two solid diamonds. Because of the current alignment and sample observation limitations, it is usually preferred to use only one perforated diamond for pressures above 20 GPa. Progress in DAC designs will likely circumvent this limitation in the future. Due to the same limitations, the pressure cannot be monitored using the standard ruby fluorescence technique.<sup>36</sup> Instead it is recommended to use gold's equation of state as an *in situ* pressure determination material. The high  $Z$  of this pressure standard provides a strong signal and its low bulk modulus provides sufficient pressure resolution for most experiments, even at high energy.

In summary, the inability with the current DAC designs to perfectly align a DAC with two perforated anvils requires us to most commonly use one perforated diamond and one solid diamond to measure amorphous diffraction at pressure beyond 20–30 GPa. With more advanced DAC alignment techniques, two perforated designs are foreseen to be able to reach the extreme pressures accessible with regular anvils. The choice of placing the perforated diamond on the upstream or on the downstream side of the sample can be argued both ways. The advantages of using the solid diamond on the downstream side and the perforated diamond on the upstream side are that the background does not change significantly with pressure and the attenuation correction is not required. If the diamonds are switched, the intensity of the background is lowered and the sample signal is more readily observed on the uncorrected pattern.

## V. EXAMPLES

We present two case studies using the method and instrumentation developed above. The first example ( $\text{SiO}_2$  glass) uses a cell with one perforated diamond on the downstream side and a solid diamond on the upstream side. The example demonstrates that by using a combination of the backgrounds collected before and after the experiment, the data can be properly corrected to the highest pressure. The pressure of the data (43.5 GPa) also demonstrates the mechanical stability of the anvils. The second example presented below is  $\text{B}_2\text{O}_3$  glass collected in a cell assembled with two perforated diamonds. The data demonstrate that high-energy diffraction experiments on amorphous materials can be performed even on extremely light amorphous materials. The quality of the data in this case clearly shows the benefit of using two perforated diamonds.

### A. Silica ( $\text{SiO}_2$ ) glass

The *in situ* study of the amorphous-amorphous transition in vitreous  $\text{SiO}_2$  at high pressure<sup>14</sup> is a challenging XRD experiment. The major structural changes in  $\text{SiO}_2$  glass occur between 20 and 50 GPa. A recent DAC XRD study of  $\text{SiO}_2$  glass to 50 GPa used regular diamond anvils and the energy dispersive diffraction technique.<sup>14</sup> We have collected a similar set of data using a monochromatic 80 keV beam and perforated DAC,<sup>37</sup> allowing an accurate measurement of the structure factor and associated analysis of structural changes in  $\text{SiO}_2$  glass at high pressure. The experiments were performed using a perforated diamond on the downstream side of the cell and a solid diamond on the upstream side. Backgrounds were collected before and after the experiment as described in Sec. III, and the downstream diamond was mounted on a c-BN backing plate. The absorption correction curve of the backing plate with the diamonds was also measured during the experiment. Using all these information, it was possible to successfully correct the data on glassy  $\text{SiO}_2$  from room pressure up to over 43 GPa. The integrated backgrounds of the cell before and after the experiment are presented in Fig. 5. In Fig. 7(b), the azimuth projection of the 2D pattern does not clearly show the diffraction pattern of  $\text{SiO}_2$  glass when compared to the background [Fig. 7(a)]. However, once the background is subtracted, the diffraction pattern from the sample becomes clearly visible [Fig. 7(c)]. The subtraction of the background pattern also removes most of the diamond peaks from the diffraction pattern. Once the background and absorption corrections have been applied, the image can be integrated into a 1D pattern. In order to remove remaining artifacts and diamond peaks in the pattern, we use the median of the pixel value of each column ( $Q$  as a function of azimuth) as the integrated value. The pattern is then free of the discretely located single crystal diamond peaks. It is only possible to extract the structure factor  $S(Q)$  if the corrections are carried out properly, otherwise the data do not oscillate around the atomic self-scattering curve at high  $Q$ . Figure 7(e) presents the  $S(Q)$  of  $\text{SiO}_2$  glass at 43.5 GPa.

### B. Boron oxide ( $\text{B}_2\text{O}_3$ ) glass

Glassy  $\text{B}_2\text{O}_3$  was measured up to 16 GPa using a DAC with two perforated diamonds. The pressure was measured using the gold equation of state.<sup>38</sup> The packed sample of vitreous  $\text{B}_2\text{O}_3$  was loaded in a gold lined hole in a rhenium gasket. The low background from the double perforated cell made the data reduction relatively straight forward, even for an extremely low  $Z$  material such as  $\text{B}_2\text{O}_3$  glass. The intensity of the diamond diffraction peaks were very weak in the background and sample pattern [Figs. 8(a)–8(c)]. Figure 8 illustrates the data reduction steps. Figure 8(a) shows the background of the empty cell. The background is not as “clean” as in the  $\text{SiO}_2$  experiment and shows traces of a weak crystalline pattern matching that of the rhenium gasket. The rhenium pattern was observed in both the background and the sample scattering. Since the data are collected at high energy and the bulk modulus of rhenium is high, there is no measurable shift in the rhenium peaks within the experimen-

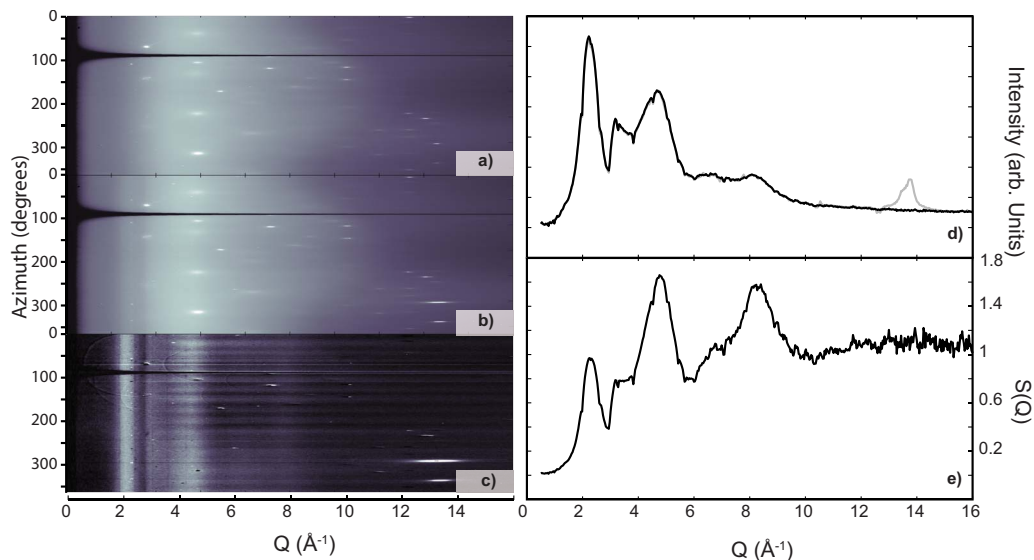


FIG. 7. (Color online) Illustration of the data reduction process for the 2D XRD pattern of a vitreous  $\text{SiO}_2$  sample in the perforated DAC with one perforated diamond on the downstream side and one solid diamond on the upstream side of the cell *in situ* at 43.5 GPa. Images (a)–(c) are a projection of the polar 2D XRD pattern into a 2D image, where the Y axis is the azimuth direction. The images presented here are generated using a simple MATLAB program but could also be formed using the freely available FIT2D software program (Ref. 31). The images are (a) the combined background composed of a ratio of the empty cell background collected before compression and the empty cell background collected after decompression from 43.5 GPa, (b) the raw measured XRD data, and (c) the glassy  $\text{SiO}_2$  data after background subtraction and absorption correction. On the right, (d) shown in light gray is the integrated pattern using the mean of the intensity as a function of azimuth for each  $Q$  and in black integrated pattern using the median of the intensity as a function of azimuth for each  $Q$ . The median function removes the diamond peaks and spurious scattering measured by the detector. Plot (e) is the structure factor  $S(Q)$  after the self scattering and Compton corrections are removed and divided by the average scattering to obtain pseudonuclear x-ray function.

tal pressure range ( $<16$  GPa). As a result, the background-subtracted scattering is free of the rhenium diffraction peaks and the signal from the sample itself is clearly visible. The intensity of the background used for the absorption correction was weak when using perforated diamonds, and as a

result, some artifacts [black lines in Fig. 8(c)] are observed in the absorption corrected 2D data. The artifacts do not change the resulting integrated corrected pattern as we use the median of the intensity in each column of the azimuth projection to obtain the 1D integrated pattern.

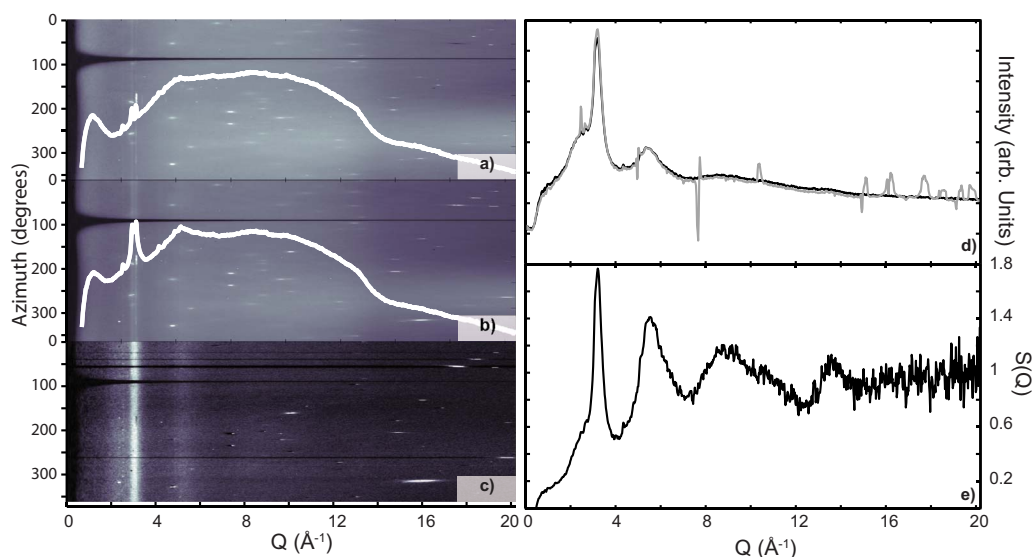


FIG. 8. (Color online) Illustration of the data reduction for a 2D XRD pattern of  $\text{B}_2\text{O}_3$  glass at 16 GPa in the perforated DAC loaded with two perforated diamonds. Images (a)–(c) are a projection of the polar 2D XRD pattern into a 2D image where the Y axis is the azimuth. The images presented here are generated using a simple MATLAB program but could also be formed using the freely available FIT2D software program (Ref. 31). The images are (a) the combined background composed of a ratio of the empty cell background collected before compression and the empty cell background collected after decompression from 16 GPa overlaid with the median of all the azimuth patterns in white, (b) the raw measured XRD data overlaid with the median of all the azimuths pattern in white, and (c) the glassy  $\text{B}_2\text{O}_3$  data after background subtraction and absorption correction have been applied. On the right, (d) shown in light gray is the integrated pattern using the mean of the intensity as a function of azimuth for each  $Q$  and in black integrated pattern using the median of the intensity as a function of azimuth for each  $Q$ . The median function removes the diamond peaks and spurious scattering measured by the detector. Plot (e) is the structure factor  $S(Q)$ .

## VI. CONCLUSIONS

In summary, we have shown that by using laser-drilled diamonds with narrow perforations, it is possible to measure high quality high-energy x-ray scattering of light amorphous materials. The choice of one or two perforated diamond is made depending on the materials and the experimental pressure range desired. With advances in DAC designs, we are expecting that the use of two perforated diamonds will become a routine for most experiments requiring low background.

## ACKNOWLEDGMENTS

This work was supported in part by the National Nuclear Security Administration Carnegie/DOE Alliance Center (NNSA CDAC). Use of the Advanced Photon Source at Argonne National Laboratory was supported by the U.S. Department of Energy, Office of Science, Office of Basic Energy Sciences, under Contract No. DE-AC02-06CH11357. We would also like to thank Dr. Malcolm Guthrie for helpful discussions and Dr. Guoyin Shen for lending us the c-BN backing plates.

- <sup>1</sup>C. E. Weir, E. R. Lippincott, A. Van Valkenburg, and E. N. Bunting, *J. Res. NBS A Phys. Chem.* **63A**, 55 (1959).
- <sup>2</sup>R. J. Hemley and H. K. Mao, *Miner. Mag.* **66**, 791 (2002).
- <sup>3</sup>R. J. Hemley, H. K. Mao, and V. V. Struzhkin, *J. Synchrotron Radiat.* **12**, 135 (2005).
- <sup>4</sup>W. A. Bassett, *High Press. Res.* **29**, 163 (2009).
- <sup>5</sup>K. Brister, *Rev. Sci. Instrum.* **68**, 1629 (1997).
- <sup>6</sup>R. L. Smith and Z. Fang, *J. Supercrit. Fluids* **47**, 431 (2009).
- <sup>7</sup>S. Matsumura, M. Watanabe, A. Mizuno, and S. Kohara, *J. Am. Ceram. Soc.* **90**, 742 (2007).
- <sup>8</sup>M. C. Wilding, C. J. Benmore, and J. K. R. Weber, *J. Mater. Sci.* **43**, 4707 (2008).
- <sup>9</sup>M. C. Wilding, C. J. Benmore, J. A. Tangeman, and S. Sampath, *Europhys. Lett.* **67**, 212 (2004).
- <sup>10</sup>W. A. Crichton, M. Mezouar, T. Grande, S. Stolen, and A. Grzechnik, *Nature (London)* **414**, 622 (2001).
- <sup>11</sup>J. H. Eggert, G. Weck, P. Loubeyre, and M. Mezouar, *Phys. Rev. B* **65**, 174105 (2002).
- <sup>12</sup>M. Guthrie, C. Tulk, C. Benmore, J. Xu, J. Yarger, D. Klug, J. Tse, H. Mao, and R. Hemley, *Phys. Rev. Lett.* **93**, 115502 (2004).
- <sup>13</sup>Y. Katayama, T. Mizutani, W. Utsumi, O. Shimomura, M. Yamakata, and K. Funakoshi, *Nature (London)* **403**, 170 (2000).
- <sup>14</sup>C. Meade, R. Hemley, and H. Mao, *Phys. Rev. Lett.* **69**, 1387 (1992).
- <sup>15</sup>Q. Mei, C. J. Benmore, E. Soignard, S. Amin, and J. L. Yarger, *J. Phys.: Condens. Mater.* **19**, 415103 (2007).
- <sup>16</sup>Q. Mei, R. Hart, C. Benmore, S. Amin, K. Leinenweber, and J. Yarger, *J. Non-Cryst. Solids* **353**, 1755 (2007).
- <sup>17</sup>M. Mezouar, P. Faure, W. Crichton, N. Rambert, B. Sitaud, S. Bauchau, and G. Blattmann, *Rev. Sci. Instrum.* **73**, 3570 (2002).
- <sup>18</sup>J. Parise, S. Antao, F. Michel, C. Martin, P. Chupas, S. Shastri, and P. Lee, *J. Synchrotron Radiat.* **12**, 554 (2005).
- <sup>19</sup>G. Shen, V. Prakapenka, M. Rivers, and S. Sutton, *Rev. Sci. Instrum.* **74**, 3021 (2003).
- <sup>20</sup>E. Soignard, S. A. Amin, Q. Mei, C. J. Benmore, and J. L. Yarger, *Phys. Rev. B* **77**, 144113 (2008).
- <sup>21</sup>K. Tsuji, K. Yaoita, and M. Imai, *Rev. Sci. Instrum.* **60**, 2425 (1989).
- <sup>22</sup>A. Yamada, T. Inoue, S. Urakawa, K.-I. Funakoshi, N. Funamori, T. Kikegawa, H. Ohfuji, and T. Irifune, *Geophys. Res. Lett.* **34**, L10303, doi:10.1029/2006GL028823 (2007).
- <sup>23</sup>K. Yaoita, Y. Katayama, K. Tsuji, T. Kikegawa, and O. Shimoda, *Rev. Sci. Instrum.* **68**, 2106 (1997).
- <sup>24</sup>L. Ehm, S. M. Antao, J. Chen, D. R. Locke, F. M. Michel, C. D. Martin, T. Yu, J. B. Parise, S. M. Antao, P. L. Lee, P. J. Chupas, S. D. Shastri, and Q. Guo, *Powder Diffr.* **22**, 108 (2007).
- <sup>25</sup>K. W. Chapman, P. J. Chupas, G. J. Halder, J. A. Hriljac, C. Kurtz, B. K. Greve, C. J. Rushman, and A. P. Wilkinson, "Optimizing high-pressure pair distribution function measurements in diamond anvil cells," *J. Appl. Crystallogr.* (in press).
- <sup>26</sup>Contact [info@almaxindustries.com](mailto:info@almaxindustries.com).
- <sup>27</sup>W. Bassett, A. Anderson, R. Mayanovic, and I. Chou, *Z. Kristallogr.* **215**, 711 (2000).
- <sup>28</sup>W. Bassett, A. Anderson, R. Mayanovic, and I. Chou, *Chem. Geol.* **167**, 3 (2000).
- <sup>29</sup>A. Dadashev, M. Pasternak, G. Rozenberg, and R. Taylor, *Rev. Sci. Instrum.* **72**, 2633 (2001).
- <sup>30</sup>S. M. Seltzer, *Radiat. Res.* **136**, 147 (1993).
- <sup>31</sup>A. P. Hammersley, S. O. Svensson, M. Hanfland, A. N. Fitch, and D. Häusermann, *High Press. Res.* **14**, 235 (1996).
- <sup>32</sup>A. Leadbetter and A. Wright, *J. Non-Cryst. Solids* **7**, 141 (1972).
- <sup>33</sup>A. Mukai, S. Kohara, and T. Uchino, *J. Phys.: Condens. Mater.* **19**, 455214 (2007).
- <sup>34</sup>P. J. Chupas, K. W. Chapman, and P. L. Lee, *J. Appl. Crystallogr.* **40**, 463 (2007).
- <sup>35</sup>E. Soignard and P. F. McMillan, in *High-Pressure Crystallography*, Mathematics, Physics and Chemistry, edited by A. Katrusiak and P. F. McMillan (Kluwer Academic, Amsterdam, 2003), Vol. II, p. 81.
- <sup>36</sup>H.-K. Mao, J. Xu, and P. Bell, *J. Geophys. Res.* **91**, 4673, doi:10.1029/JB091iB05p04673 (1986).
- <sup>37</sup>C. J. Benmore, E. Soignard, S. A. Amin, M. Guthrie, S. D. Shastri, P. L. Lee, and J. L. Yarger, *Phys. Rev. B* **81**, 054105 (2010).
- <sup>38</sup>S.-H. Shim, T. S. Duffy, and K. Takemura, *Earth Planet. Sci. Lett.* **203**, 729 (2002).